How far the Chemistry of the Self-Assembly Monolayers on Gold Surfaces Affects their Work Function?

Léo Bossard-Giannesini, Luis Cardenas, Hervé Cruguel, Aude Demessence, David Loffreda, Olivier Pluchery

Nanoscale

ARTICLE

How Far the Chemistry of Self-Assembled Monolayers on Gold Surfaces Affects Their Work Function?

Received 00th January 20xx,
Accepted 00th January 20xx

DOI: 10.1039/x0xx00000x

www.rsc.org/

Léo Bossard-Giannesini, [a] Luis Cardenas [b], Hervé Cruguel [a], Aude Demessence [b], David Loffreda *[c] and Olivier Pluchery *[a]

Abstract. Self-assembled monolayers composed of various long-chain aliphatic molecules and different tail functional groups have been synthesized on the Au(111) surface and characterized by Kelvin Probe Force Microscopy and Ultraviolet Photoelectron Spectroscopy. Carboxy, amino, thio and methyl terminal groups have been considered in the design of self-assembled monolayers with different aliphatic chain lengths (from C6 to C16). The work function measurements by Kelvin Probe Force Microscopy have been carried out under controled and room atmosphere. Remarkably, a reduction of the relative humidity from 40 % to 3 % has induced a work function shift up to 0.3 eV. As expected, the changes of the chain length of the aliphatic moiety and of the tail group have a significant impact on the tuning of the measured work function (3.90 eV for dodecanethiol versus 4.57 eV for mercaptohexadecylamine). Surprisingly, the change of the net dipole moment of the tail group (sign and amplitude) does not dominate the work function variations. In contrast, the change of the chain length and the possibility of the tail group to form a complex hydrogen-bond network between molecules, lead to significant modulations of the work function. In order to interpret these original findings, density functional theory models of equivalent self-assembled monolayers adsorbed on the Au(111) surface have been developed at an unprecedented level of description with large supercells including simultaneously 27 coadsorbed molecules and weak van der Waals interactions between them. Such large systems have allowed the theoretical modeling of complex hydrogen-bond networks between molecules when possible (carboxy tail group). The comparison between computed and measured work functions shows a striking agreement, thus allowing the disentanglement of the previously mentioned competing effects. This consistency between experiment and theory will help designing the electronic properties of self-assembled monolayers in the context of molecular electronics and organic transistors.

.

Introduction

Alkanethiols represent a class of ideal molecules for building robust and reproducible functionalized gold surfaces. Interestingly, self-assembled monolayers (SAM) enable adding new functionalities to a gold surface for building biosensors,[1, 2] modulating the surface electric properties,[3-7] and opening new perspectives for molecular devices.[8, 9] Several reviews report on the numerous studies devoted to the morphology of SAMs on various metals.[10-12] Among the interesting molecules, dodecanethiol has been investigated in details and the corresponding SAMs arrange into a *brush-like* structure with the sulfur moiety strongly bound to gold.[13-16] This SAM is terminated by the methyl group, which makes the coated metallic surface fairly passive towards further reactions and other functionalizations. Other tail groups than CH_3 were also studied, such as carboxy, alkoxy, amino or thio groups[17-20] or fluorinated tail groups.[21-23] Very active debates have appeared in the literature related to the change of this substituent and the subsequent modulation of the electrostatic properties of metallic surfaces.[24-28] Among these properties, the work function (WF) is the most emblematic one. It is defined for a surface as the required energy for extracting one electron from the Fermi level of the metal to the vacuum level, far from the surface. Such definition is adequate for ideal planar surfaces of homogeneous materials.[29, 30] In molecular science, it is a concept similar to the ionization energy (IE) (see for example, critical comparison of WF and IE in Ref[31]). IE and WF are playing central roles in the understanding of many fundamental mechanisms, in terms of chemical reactivity, photocatalysis, or nanoelectronics. Measuring values for the WF of functionalized surfaces has been carried out with various techniques: Ultraviolet Photoelectron Spectroscopy (UPS) under vacuum conditions, Kelvin Probe and more recently, Kelvin Probe Force

[a] Institut des NanoSciences de Paris, UMR7588 CNRS Sorbonne Université, 4 place Jussieu, 75005 Paris, France.
[b] Université de Lyon, Université Claude Bernard Lyon 1, CNRS, IRCELYON - UMR 5256, 2 Avenue Albert Einstein, 69626 Villeurbanne, France.
[c] ENSL, CNRS, Laboratoire de Chimie UMR 5182, 46 Allée d'Italie, 69364 Lyon Cedex, France.
* Corresponding authors: olivier.pluchery@insp.jussieu.fr, david.loffreda@ens-lyon.fr
† Footnotes relating to the title and/or authors should appear here.
Electronic Supplementary Information (ESI) available: [details of any supplementary information available should be included here]. See DOI: 10.1039/x0xx00000x

Microscopy (KPFM) in atmosphere or in vacuum.[21, 22, 32, 33] Knowing the WF is critical for devices, it has also been measured in various contexts including electric characterization of barrier heights in junctions, such as metal-organic interfaces,[8, 9, 21] light-emitting devices (LED),[6] or field emission guns.[34] For example, in the case of the most widely studied SAM, such as dodecanethiol on Au(111), the effective WF was measured mostly with UPS between 3.9 and 4.1 eV.[5, 34, 35] Debates in the literature call for a rationale of the WF predictions. In this context, it is tempting to evaluate the WF of functionalized surfaces by considering the dipole moment of the free molecules. It is known that the WF of a surface *increases* when it is covered with a sheet of *inwards* dipoles and *decreases* with *outwards* dipoles.[36, 37] Let's denote μ_z the z-component of the electrostatic dipole perpendicular to the surface, the Helmholtz formula expresses the modification of the WF as follows:

$$\Delta WF = -\frac{\mu_z}{\varepsilon_0 A} = -\frac{q \cdot d}{\varepsilon_0 A} \qquad (1)$$

where *A* is the area occupied by one molecule, $\pm q$ corresponds to two opposite charges positioned at a distance *d* from each other. This electrostatic approach is discussed in depth by Heimel.[36, 37] Thus, we can consider a realistic SAM made of molecules organized as a square lattice of parameter a = 0.2 nm. If each molecule bears a dipole of −1.0 D which corresponds to $q = \pm e/10$, and a charge separation $d = 0.2$ nm, this SAM would generate a very large WF change of +9.0 eV.[37] This pure electrostatic approach predicts ΔWF values that are ten times larger than the typical experimental values, and is probably too simplified. Other contributions play a major role, such as the highly polar molecule-surface bond,[24, 38] or a depolarization factor due to the compression of molecules in monolayers which decreases the impact of the initial molecular dipole.[39] More elaborated theoretical models describing the chemical bonding have been reported in the literature based on density functional theory (DFT) and quantum mechanics. Several approaches were proposed either by calculating the resulting dipole of a floating molecular sheet[8] or by developing a more realistic SAM in interaction with gold.[24, 25, 36] More recently, Van der Waals interactions between the molecular chains were also included in the DFT models with various functions.[20, 40-44] The considered supercells aiming to describe the SAM on gold are usually rather small in order to significantly reduce the computational cost, thus restricting the exploration of the complex relative conformations and orientations of the coadsorbed molecules at long range. In addition, in experimental conditions the presence of contaminants adds a supplemental and hardly incontrollable dipole contribution that blurs the WF values.[3] It results that the effective WF modification of a thiol-covered gold surface may depend on the following factors: (1) the permanent dipole of the isolated molecule, that can be adjusted by modifying the tail group, (2) the molecule chain length, (3) the surface packing density (4) the polarity of the gold-sulfur bond and (5) the presence of polar contaminants.

The aim of the present work is to provide a detailed study of the modification of the WF of reconstructed Au(111) gold surfaces when they are functionalized by alkylthiol molecules with different chemical terminations. The SAM formation is investigated with two experimental techniques and a set of state-of-the-art DFT calculations allowing the exploration of complex coadsorption motifs with large supercells and a large number of molecules. Four terminal groups are addressed: methyl, carboxyl, amino, and thio (see Figure 1). We also discuss the effect of the chain length. We show that the WF is systematically decreased compared to bare gold, even with molecules exhibiting a strong inward dipole in their free state.

Experimental

Gold surface preparation.

Evaporated gold. Gold surfaces are obtained by thermally evaporating 200 nm of pure gold on a glass substrate (microscope slide from Menzel Gläser) without any adhesion layer, under vacuum (3 x 10^{-6} mbar). The glass substrate was first degreased with acetone and ethanol. The resulting evaporated gold surface was rinsed with absolute ethanol (99.9 %) and dried with a nitrogen flow.

Reconstructed gold. Evaporated gold surfaces were reconstructed under a propane flame during 30 s. The control of the *flaming temperature* is important and is achieved by ensuring a homogeneous orange color of the surface in a completely dark room. This surface was then cooled down and rinsed copiously with absolute ethanol during 30 s. A drop of ethanol was left for protecting the surface from air contamination before functionalization. For the study of the reconstructed gold, the surface was dried under a nitrogen flow. This experimental protocol is well documented and is known to produce facets of (111) orientation on gold.[19, 45, 46]

Functionalization of the gold surfaces. Reconstructed gold surfaces were functionalized with thiol molecules in order to form the SAMs. Four types of thiols are used: 8-amino-1-octanethiol (**AOT**) (98.5 %), 16-mercaptohexadecanoic acid (**MHDA**) (99 %), 1,6-hexanedithiol (**HDT**) (97 %) and dodecanethiol (**DDT**) (98 %) (Figure 1-a). All compounds were purchased from Sigma-Aldrich. SAMs were deposited on freshly prepared gold surfaces by covering the surface with the solutions. Thiol solutions were prepared in absolute ethanol with a concentration of 10 mM for AOT, MHDA and DDT, and a concentration of 1 mM for HDT. The immersion time is of 90 min for AOT, MHDA and DDT, and 30 s for HDT. In the case of HDT, this short immersion time was selected to avoid the formation of disulfide bridges between tail groups. Notice that if disulfide bridges are formed, they can be detected with STM as parallel linear motifs in the SAM.[19] These parameters enabled a complete saturation of the surface by the molecules. Surfaces were then dried under a nitrogen flow.

Kelvin Probe Force Microscope.

Topography and contact potential differences (CPD) were measured simultaneously with a commercial Kelvin probe force microscope (KPFM, Multimode 8, Bruker) in a dual pass mode.

The CPD channel is acquired within the AM (amplitude modulation) mode and with an accuracy of 5 mV. Topography is acquired with the Peakforce® mode which allows controlling the interacting force with the surface and preserves the tip sharpness. KPFM was recorded at room temperature in a humidity controlled environment where the relative humidity (RH) was adjusted between 3 % and 40 % (room atmosphere). RH was controlled by flowing ultrapure nitrogen gas into the KPFM sealed compartment.

Ultraviolet-Photoemission Spectroscopy.

UPS analysis was carried out in an integrated commercial ultrahigh vacuum photoemission system Axis ULTRA DLD spectrometer. UPS spectra were obtained using a helium ionization lamp with two resonances lines, He I at 21.2 eV and He II at 40.8 eV. To calibrate the work function of the analyzer, a negative bias potential of 9.1 V was applied to the sample. Prior to measurements, an Ag foil was cleaned by argon ion sputtering. The bias was optimized to shift the Ag spectrum in the linear region of the analyzer (0–10 eV kinetic energy).[47] A work function of 4.2 eV was obtained, in agreement with the literature value of 4.26 eV.[48, 49] The WF on each surface was calculated using the energy cutoff obtained from the first derivative of the UPS spectrum ($\phi = E_{cutoff} \pm 21.2$ eV) .

WF calculations with DFT modelling.

In this study, Density Functional Theory calculations were performed with the VASP 5.4 package.[50-52] The electronic exchange-correlation GGA PBE functional[53] was considered in combination with the semi-empirical dispersion-correction method DFT-D3 in its zero-damping formalism.[54] The interactions between electrons and ion cores were described by potentials generated by the Projector Augmented-Wave method (PAW potentials, 11 valence electrons per gold atom).[55] Valence electrons were expanded in plane waves with a kinetic cutoff energy of 400 eV (in the range 7263-9315 valence electrons depending on the molecule). A large p(9x9) supercell of a Au(111) slab composed of 7 atomic planes was used (corresponding to a hexagonal box with lattice vectors of lengths 25.92×25.92×49 Å^3) with adsorption of various SAM on one side of the slab (non-symmetric adsorption). A large vacuum space along z-axis (in the range 12.8-27.3 Å according to the molecule) was described in order to avoid spurious interactions between the adsorbate and the other side of the periodic metallic slab. Five different molecules (see Figure 1-b) were adsorbed on the Au(111) slab through the best adsorption structure (top site through S atom of the SH moiety). The thiol molecules were adsorbed molecularly on the gold surface since a previous theoretical study showed that dissociative adsorption of long alkyl chain thiols (leading to thiolates) is not favored.[15] SAMs of these molecules were generated by co-adsorbing 27 molecules in the p(9x9) supercell leading to a (√3x√3)-R30°-27thiol adlayer motif (see Figure 6-a). The chosen surface coverage of 1/3 ML (monolayer) corresponds to adlayers close to saturation, as depicted in Figure 6 for the SAM of MHDA and Figure 7 for other SAMs. Due to the selected large supercell, the Brillouin zone sampling in reciprocal space was restricted to the Γ point ensuring a good convergence of the total electronic energy. For Au bulk, the grid of Brillouin zone used for determining accurate total electronic energy was 39×39×39 k-points, thus giving an optimal lattice parameter a_0 of 4.0727 Å (in close agreement with measurements: 4.0783 Å) and cohesion energy of −3.69 eV/at. (also in fair agreement with experiments, −3.81 eV/at.). For dealing with the partial occupancies around the Fermi level, a Methfessel–Paxton smearing was used with σ = 0.2 eV. The geometry optimizations were completed by relaxing entirely the degrees of freedom of the adlayers and of the metallic planes, with a convergence criterion of 10^{-6} eV for the total electronic energy, until each residual force on nuclei was less than ±0.01 eV.Å^{-1}. The calculations of the work function were based on the predictions of the electrostatic potential. For each SAM on Au(111), the integrated potential in the (x,y) plane was predicted by single-point energy calculations on the basis of previously optimized structures and plotted along the z axis, in much more accurate computational conditions (kinetic energy cutoff of 500 eV and a vacuum space systematically increased by 10 Å along the z axis to help the convergence of the vacuum level). The WF (positive value) was then derived by the difference between the position of the vacuum (positive value) and the Fermi level (negative value) (see Table 2). The systematic error of the computed work function has been estimated by changing the thickness of the gold slab from 3 to 7 layers and has a value ±31 meV.

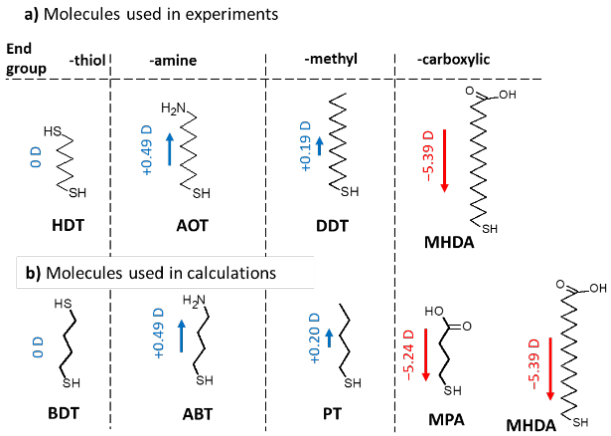

Figure 1. Molecules used for the SAM formation on gold surfaces for a) the experiment and b) the DFT calculations. Four types of molecules are used differing by their end group: thiol moiety for hexanedithiol (**HDT**) and butanedithiol (**BDT**), amine moiety for aminooctanetiol (**AOT**) and aminobutanethiol (**ABT**), methyl moiety for dodecanethiol (**DDT**) and pentanethiol (**PT**), or carboxylic moiety for mercaptoundecanoic acid (**MHDA**). and mercaptopropanoic acid (**MPA**). The resulting permanent dipole of the isolated molecule is also indicated and expressed in debye, as calculated with the Hückel approach (in blue when positive and in red when negative).

Results

CPD of bare and functionalized gold

First, the morphology of the gold surfaces before the functionalization was investigated. With KPFM, the evaporated gold surfaces exhibit a uniform morphology (Figure 2-a) but their potential is not homogeneous as shown in Figure 2-b. On 2x2 µm² images, important drops of potentials of 100 mV were observed due to adventitious adsorbates and local surface defects. In the following, systematic flame annealing was performed in air, followed by a rinsing with ultrapure ethanol, in order to yield a reconstructed surface. With this method we obtained morphologically flat surfaces and large terraces of

400 nm, with a homogeneous potential (< 5 mV variations) and stronger contrasts (50 mV) at the step edges as visible in Figure 2-c) and d).
After SAM formation with the four molecules, the terraces are preserved.

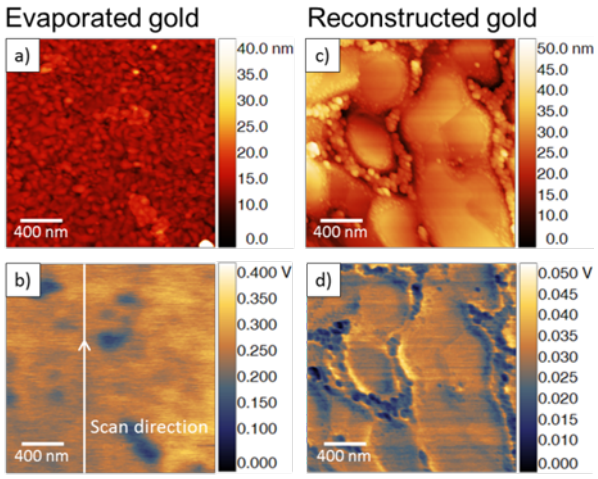

Figure 2: AFM-KPFM images (2x2 µm²) of bare gold surfaces: evaporated gold with a) topography and b) CPD map, and reconstructed gold with c) topography and d) CPD map. The image is recorded line by line and thus allows a potential measurement as a function of time.

Impact of the relative humidity on the WF. After the SAM formation, the evolution of the CPD as a function of RH was monitored. KPFM images were acquired line by line and in Figure 3, the average of the CPD values over each line is plotted as a function of time (grey line), simultaneously with the RH (green dotted line). We can distinguish three regions: region **I** is just after the SAM formation, region **II** is 2 h after the SAM formation and region **III**, 24 h later. During these 24 h, the sample was in contact with the ambient atmosphere. These three time-delays correspond roughly to three typical durations when the samples are manipulated in atmosphere: delay **I** is the quickest delay between the end of the chemical preparation and the first CPD measurement. Delay **II**, is the duration of an average KPFM experiment session for one sample and delay **III** is considered as the stabilized surface. In Figure 3 the CPD of the reconstructed gold surface functionalized with a SAM of HDT is presented. We can observe two phenomena. First, the potential evolves towards more positive values, with time and with the ambient atmosphere: from −0.33 V to +0.05 V. Then the introduction of N_2 and the decrease of humidity to 3 % do not restores the potential to the starting value, but it slows down the evolution. Finally, a stability is reached after 24 h (part III). From the deposition of the SAM to the stability after 24 h, the potential has increased by 0.38 V. The four SAM studied in this article present a similar behavior with albeit different kinetics and different amplitudes (see a summary in Figure 4).

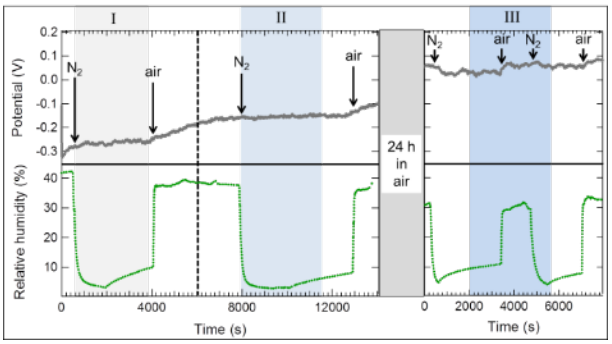

Figure 3: evolution of the measured potential (grey curve) of a HDT SAM on gold as a function of time. The relative humidity measured in real time in the box is also shown (green dotted line). Corresponding introduction of N_2 or air in the box is also indicated.

CPD of each SAM and calibration of the WF. CPD values are directly obtained from the KPFM images. CPDs are relative values, defined by $V_{CPD} = 1/e\left(WF_{sample} - WF_{tip}\right)$ where e is the elementary charge (positive value). In our experiment the bias is applied to the surface, therefore an increase of the WF of the sample results in an increase of the measured CPD.[32, 56] The conversion of CPDs into an absolute value of the WF requires a calibration, which is far from simple.[32] In the present case, calibration is carried out with a reference sample made of aluminum, covered with an alumina thin oxide. This surface exhibits a stable WF in air of 4.55 eV.[57] Results are presented in Figure 4. The calibration was achieved by systematically measuring the aluminum surface before and just after recording the images of the functionalized surface of interest. This allows detecting the possible change of the WF of the tip during an experiment. The largest variation measured was 140 mV. Therefore, the uncertainty of the measured WF in this study is ±70 meV.
The surface of evaporated gold evolves from 4.72 eV to 4.80 eV in 24 h. The flamed gold surface exhibits a WF of 4.87 eV and the time evolution was not monitored. For the MHDA SAM, the WF increases regularly with time of about 0.30 eV within a day in air. Gold surfaces functionalized with AOT and HDT evolves in a very similar way from an initial value of 4.28 eV and a slow increase to 4.74 and 4.91 eV, respectively. This is not the object of the present work to discuss the reason of these evolutions strongly related to the water molecules.[58] Finally, the DDT SAM exhibits the lowest WF among the SAMs in our study, at 3.90 eV. This value agrees well with those reported in literature.[5, 34, 35]

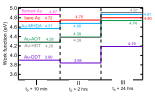

Figure 4: evolution of the WF of functionalized gold surfaces as a function of the contact time with the ambient atmosphere. WF values were obtained with calibrated KPFM measurements. Measures I are carried out in a controlled (dried) atmosphere or 3% RH. For measures II and III the samples have been exposed to air for at least 1 hour.

These data show that the WF of the freshly prepared SAMs (delay **I**) provide the most meaningful values. They are summarized in Table 1 and will be discussed and compared with those obtained with UPS and DFT.

UPS measurements and WF of SAM surfaces.

The WF measurements with photoelectron spectroscopy were carried with a special attention to some specific requirements. First of all, the incident photon energy has to exceed the WF of the sample. The WF of the analyzer and the sample were compensated by applying a constant potential during the measurement. In the case of a metal-semiconductor contact, the Fermi level of both surfaces are aligned under thermodynamic equilibrium conditions. Therefore, according to the Schottky-Mott principle, a redistribution of the charges takes place, which results into the formation of a dipole Δ at the interface.[59, 60] UPS probes an area of the surface of *ca*. 1 mm of diameter and gives therefore access to the spatially averaged value of the WF.

Figure 5 displays the two spectral regions of interest in the UPS spectra: the first region (a) is dominated by the *secondary* electrons (SEC) near the cutoff energy E_{Cutoff}. After their extraction from the surface, these photoelectrons are emitted with a kinetic energy between 1 and 10 eV, which is their remaining energy after multiple inelastic scattering events. The electrons probe a depth of a few nanometers below the surface. Nevertheless, the secondary electrons retain the initial information (escape energy), and eventually provides the value of WF. In contrast, Figure 5-b shows the spectral region of the *primary* photoelectrons, which do not undergo inelastic scattering. They represent, in a first approximation, the density of states of the material, and therefore their energies correspond to the electron binding energies.

To facilitate the calibration of the energy scale and of the Fermi level, a gold foil was cleaned through a sequence of ion sputtering with ionic argon energy of 1KeV. The UPS spectrum of this pristine gold foil (Figure 5-a, bottom spectrum) shows the excited electronic states observed as a hybridized flat band related to the *d* and *s/p* states located between E_F and ≈ 1.8 eV.[61] Subsequently, the *d* electronic states of polycrystalline gold are located between ≈ 2 eV and 8.5 eV. The WF was calculated with the assistance of the cutoff energy (E_{cutoff}) obtained from the first derivative of the SEC spectrum. The WF for pristine gold is 5.1 eV, in good agreement with the literature value.[59] Therefore, based on Fermi level alignment between Au and SAMs, one can use the reminiscent states (including E_F) of gold observed in the different spectra to calibrate each of them. This is particularly visible for the localized state at 6 V and the E_F = 0 eV, which are observed in every spectrum, excepted for MHDA. However, the broad feature observed on MHDA around 6 eV fit with both states that are visible on gold pristine at ≈6 eV and ≈4.3 eV. The emergence of these Au electronic states depends on the homogeneity and coverage rate of the Au surface by SAMs.

This calibration methodology validates the visible interface dipole Δ in the E_{cutoff} region of each UPS spectra (SAMs/Au), which varies between ±0.4 eV and ±0.9 eV forming an interface dipole barrier.[62] It plays an essential role in the direction of electron transfer in the SAM-Au junction, and thus Δ can be used as a predictive parameter.[63] The interface dipole Δ is simply related to the change of the WF, ΔWF upon adsorption by $\Delta WF = -\Delta$. The results are reported in Table 1.

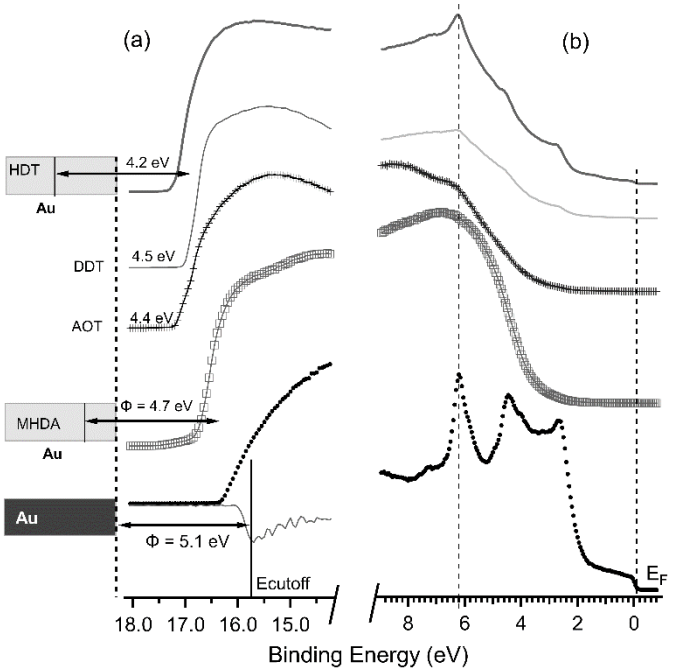

Figure 5: UPS spectra of (a) SEC and (b) primary band regions corresponding to Au, MHDA, AOT, DDT, and HDT, respectively.

Experimental values of the WF of SAM on reconstructed Au(111)				
	KPFM		UPS	
Molecule	ΔWF (V)	WF (eV)	ΔWF (V)	WF (eV)
Flamed gold	0	4.87	0	5.1
HDT Hexanedithiol	−0.59	4.28	-0.90	4.2
AOT Amino-octanethiol	−0.59	4.28	-0.70	4.4
DDT Dodecanethiol	−0.97	3.90	-0.60	4.5
MHDA Mercapto-hexadecanoic acid	−0.30	4.57	-0.40	4.7

Table 1. Experimental values for the WF obtained with KPFM and with UPS. KPFM values are those obtained immediately after surface preparation (in the time delay **I** at 3 % RH). The values of ΔWF correspond to the decrease of the WF after the gold surface is functionalized by one of the four molecules. The KPFM values of the WF are calculated using the reference surface of aluminum (WF = 4.55 eV). The WF values obtained with UPS are acquired in vacuum.

DFT calculations of the WF of SAM surfaces

To predict the variations of the WF from a theoretical approach, the SAMs of five different molecules were optimized on the basis of DFT calculations with the most accurate computational and modeling conditions: a large supercell, thick metallic slabs, a large vacuum space, a large number of co-adsorbates, high coverage close to saturation, including van der Waals weak interactions, using tight convergence criteria.

MHDA. From a computational standpoint, the most elaborated SAM of our study is this 27 MHDA that are coadsorbed molecules on Au(111) (see Figure 6 for different views and definitions). In our models, the thickness of the organic coating is almost equivalent to the thickness of the metallic slabs. The adlayer is composed of an initially perfectly distributed set of 27 MHDA molecules forming a regular checkerboard with a (√3x√3)-R30° adlayer motif (see Figure 6-a), with identical lateral orientations (*eclipsed* conformation). After geometry optimization, the SAM forms a *wavy comb* of MHDA chains (see top view in Figure 6-b). From lateral standpoints, the SAM forms either a *bent comb* (Figure 6-c) or a more regular *comb* of almost eclipsed MHDA molecules (Figure 6-d). The SAM (comb shape) is significantly inclined with respect to Au(111) as shown in Figure 6-d in agreement with previous DFT results.[20, 41] The carboxy moieties at the tail of the MHDA molecules change their initial parallel orientations during the geometry optimization, to form a discontinuous network of stabilizing hydrogen bonds between the carboxylic acids (in the range 1.75-2.45 Å) as depicted in Figure 6-e. This network constrains the bound MHDA molecules at their tails to keep an eclipsed conformation of their long hexadecyl chains. The adsorption energy per MHDA, including Van der Waals interactions, is quite strong (−2.186 eV/molec) and is largely dominated by Van der Waals interactions, also called dispersion (105 % of the covalent bonding contribution) due to the hexadecyl C16 long aliphatic chains. The increase of these long-range interactions with the length of the aliphatic chain has been previously detailed in the literature, with lengths up to C12 alkylthiol on Au111.[41] The related WF of 4.99 eV (see Table 2) is shifted to lower values with respect to the predicted WF for clean Au(111) surface (5.26 eV).[49, 64]

MPA. By considering a much shorter chain (C4 instead of C16), the corresponding SAM of MPA was modelled and optimized in equivalent conditions with respect to MHDA (see Figure 8-d, h). The adsorption strength is much weaker (-1.349 eV/molec) and less dominated by dispersion energy (86 %), although the presence of hydrogen bonds between carboxy moieties is also evidenced (notice how the almost eclipsed conformation of the MPA molecules is preserved) in agreement with Ref.[41] The decrease of the chain length also affects the WF which is shifted to lower values (4.78 eV) compared to the SAM of MHDA.

ABT. The substitution of the carboxy moieties by amino groups was then investigated by modeling the SAM of ABT on Au(111) (see Figure 8-c, g). Such a chemical change produced a concomitant decrease of the adsorption strength (-1.175 eV/molec, more dominated by dispersion: 93 %) and of the WF (4.76 eV). The absence of hydrogen bonds in this SAM offers more flexibility to optimize the relative conformation of ABT molecules thus leading to a less eclipsed configuration.

PT. At the opposite, the substitution of carboxy groups by methyl moieties gives rise to a SAM of PT molecules with a weaker adsorption strength (-1.143 eV/molec) but a larger WF (4.85 eV).

BDT. When a symmetric dithiol molecule (BDT) is used to build a SAM on Au(111), the loss of adsorption strength is more moderate (-1.224 eV/molec), while the WF is the largest one for the series of C4-chain molecules (4.87 eV). In the latter two cases (PT and BDT), no hydrogen bond network is observed likewise the SAM of ABT. This explains the more regular relative conformations of the molecules self-organized into star-like lattice.

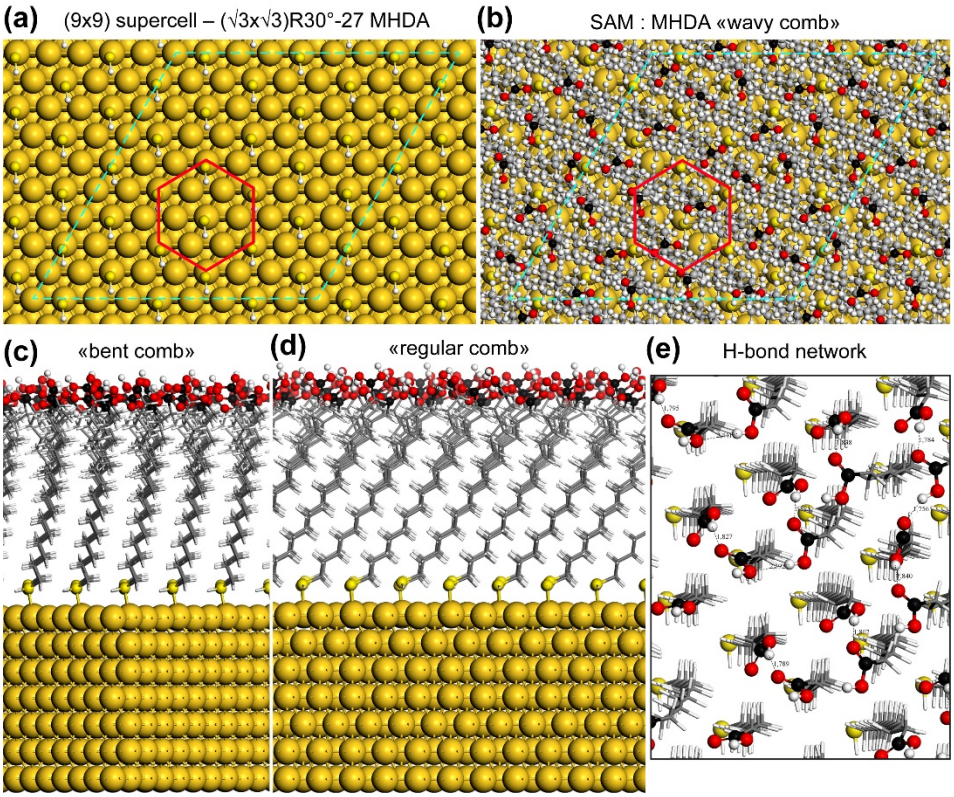

Figure 6: Different views of the optimized structure for a SAM of MHDA molecules adsorbed on Au(111) from DFT calculations : (a) top view of the Au(111) slab composed of 7 atomic layers along z axis and a (9x9) supercell in the (x,y) plane (light blue dotted lines). 27 MHDA molecules are coadsorbed in this supercell leading to a (√3x√3)-R30°-27 MHDA adlayer motif (corresponding to a molecule surface density of 4.64 molec/nm²) with a hexagonal distribution of adsorbates as shown by the red hexagon (the adsorption sites being mentioned by the positions of the SH moieties bound to Au through S atoms on top sites); (b) top view of the SAM that forms a "wavy comb" through the organization of MHDA adsorption structures; (c) lateral view of the SAM along the x axis that forms a "bent comb" through the curvature of the hexadecyl chains; (d) lateral view along y axis that forms a more "regular comb" with linear and almost eclipsed hexadecyl chains; (e) top view of the SAM by masking Au(111) and by indicating the hydrogen bonds registered between COOH moieties (distances in Å) . Au atoms are depicted with golden balls, S atoms with yellow balls, C and H atoms belonging to the hexadecyl aliphatic chains with gray and white sticks, respectively, C and H atoms of the carboxy moieties with black and white balls, respectively, O atoms with red balls.

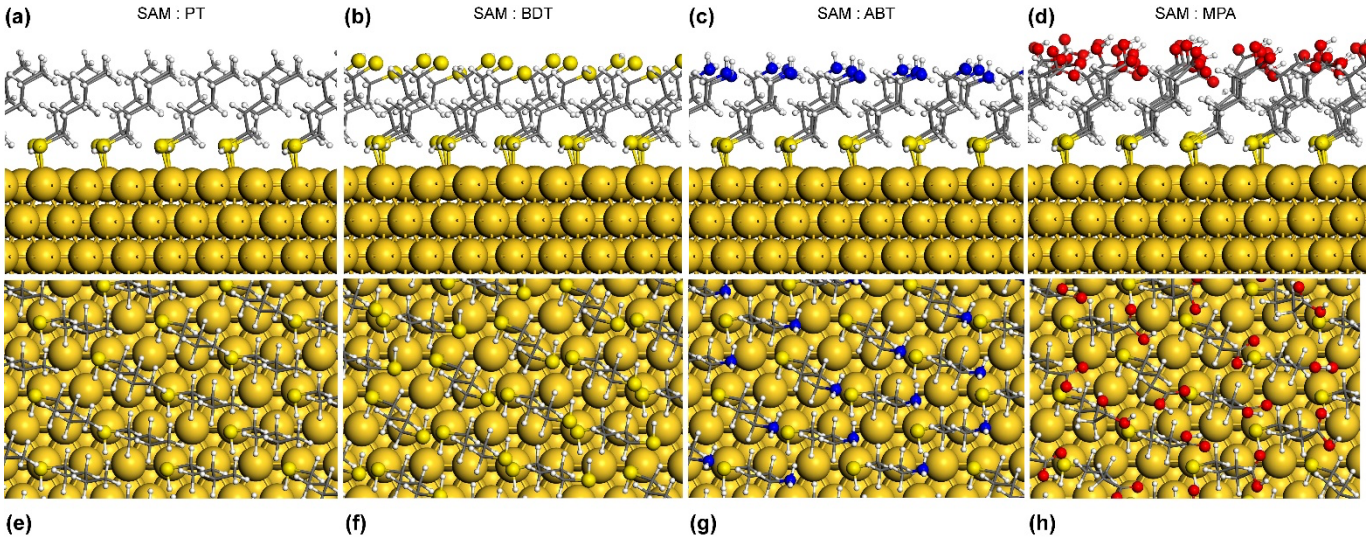

Figure 7: Different views obtained from DFT calculations of the optimized structures of four SAMs adsorbed on Au(111): lateral views of 27 coadsorbed (a) pentanethiol (PT), (b) butanedithiol (BDT), (c) aminobutanethiol (ABT), (d) mercaptopropanoic acid (MPA), and top views (e)-(h) of these SAM, respectively. The supercell, coverage and thickness of the metallic slab are identical to the SAM of MHDA exposed in Figure 6. Au atoms are depicted with golden balls, S atoms with yellow balls, C atoms with gray sticks, O atoms with red balls, N atoms with blue balls, H atoms with white balls.

Nanoscale

ARTICLE

Calculated values of the WF of SAM on Au(111)		
Molecule	**WF (eV)**	**ΔWF (eV)**
Au(111)	5.25(9)	0
MHDA Mercapto-hexadecanoic acid	4.99(2)	-0.26(7)
MPA Mercapto-propanoic acid	4.78(1)	-0.47(8)
BDT Butanedithiol	4.87(6)	-0.38(4)
ABT Amino-butanethiol	4.76(8)	-0.49(1)
PT Pentanethiol	4.85(2)	-0.40(7)

Table 2. Calculated values for the WF for the clean Au(111) surface and for five different SAMs made of MHDA, MPA, BDT, ABT and PT. **ΔWF** is the variation of the WF induced by the SAM formation, and corresponds to the values of CPD measured with KPFM.

Discussion

The Figure 8 presents a graphical summary of the experimental (a) and theoretical results (b) and will be the base of our discussion.

Absolute values of the WF. Figure 8.a) compares the WF values obtained with KPFM (colored vertical lines) and with UPS (black horizontal rods). The clean Au(111) reconstructed surface is measured at 4.87 eV with KPFM and 5.1 eV with UPS. KPFM values are systematically lower than those of UPS of ~0.2 eV. This shift has to be linked to the effects of contaminants on surfaces, namely water molecules. In vacuum the WF of Au(111) is measured at 5.33 ± 0.06 eV[49] and our calculations also predicts a WF at 5.26 eV (see Table 2). Heimel *et al.* have demonstrated that sparse dipolar molecules on a surface, such as water contamination, add an important electrostatic contribution to the overall potential energy and cause the WF to be shifted.[37]

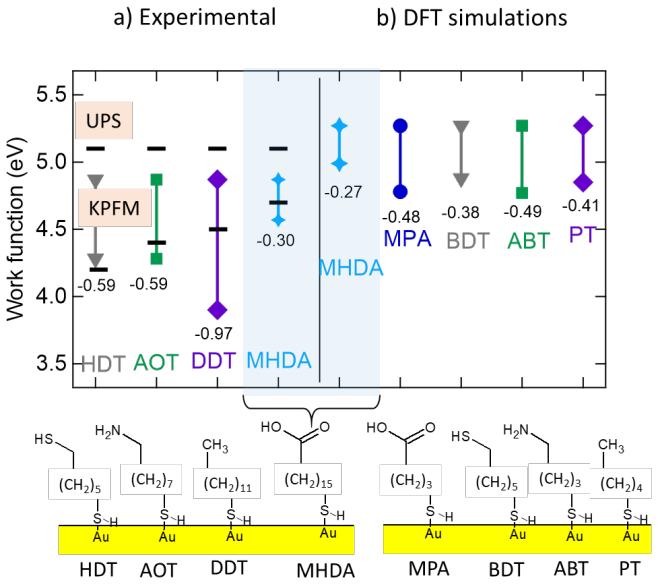

Figure 8. Work function of gold surfaces and its modification **ΔWF** upon functionalization: a) experimental values obtained from the KPFM measurements (colored vertical lines) and from UPS measurements (black horizontal rods). b) data extracted from the DFT calculations with the molecules The numerical values for **ΔWF** are indicated for each molecule on the graph.

Castanon *et al.* worked with a KPFM equipped with platinum tips and show that the presence of humidity may sometimes induce an increase of the WF of the tip of 0.6 eV, and a subsequent equivalent decrease of the WF of the sample.[58] Therefore when a sample is analyzed in air with KPFM, a lowering of the WF is expected compared to vacuum (10^{-8} mbar for UPS). We will continue our discussion by focusing on variations of WF (ΔWF). They are in good agreement for the two experimental techniques, if we exclude the molecule of DDT (see the discussion of this case below). The numerical values for these shifts in KPFM are written on Figure 8. As a partial conclusion, these data confirm that the ideally cleaned Au(111) surface has a WF of 5.26 eV. Under vacuum with a possible thin adlayer of physisorbed water, UPS detects a WF for Au(111) of 5.1 eV. Finally, when exposed to air, KPFM measures a WF of 4.87 eV for this same surface.

Is there a relation between the molecular dipole moment of the free molecule and the WF? From the Helmholtz equation (1) and from the values of the dipoles of the free molecules, one could in principle predict the values for ΔWF. For example, the monolayer of MHDA should exhibit an increase of the final WF due to the strong inward dipole of −5.39 D (see Figure 1-a). However, ΔWF of MHDA is negative with our three approaches, despite contradictory results from Lee *et al.* (WF measured at

+5.83 eV)[17]. On the same line, the HDT monolayer should induce no WF change or at least a very negligible one compared to AOT. However, our experiments show that HDT and AOT exhibit the same ΔWF of −0.59 eV. These results reveal certainly the dominating influence of other parameters than the dipole moment of the free molecule. Actually some key parameters can be listed: the polarization of Au-S bond [24, 38], the length of the molecular chain, the surface density of the molecules within the SAM, and the existence of hydrogen bonding between the tail-groups.[20] Therefore it should be concluded that the dipole moment of the free molecule has a very limited electrostatic influence on the final work function of the functionalized surface. Helmholtz equation is not wrong, but to be predictive it has to include the calculation of the resulting dipole of the adsorbed molecules and not just the dipole moment of the free molecule. Insightful results were published in the group of Zharnikov where they changed the molecular dipole of their SAM, and subsequently its WF, by either embedding different dipolar esters inside the chain molecules[26, 28] or mixing upwards and downwards dipoles.[33] With this approach, they could change the molecular dipoles without modifying too much the metal-molecule bond and they confirm that the final WF did not vary much.

Comparison between experiments and theory for MHDA. To gain insight about these shifts, the case of MHDA is interesting since this functionalization was considered with our three approaches. All these approaches conclude to a decrease of the WF yielding very close values: −0.40±0.1 eV with UPS, −0.30±0.05 eV with KPFM and −0.27±0.03 eV with DFT. This agreement validates our DFT approach which will thus be useful for analyzing the various contributions to the WF. Due to the computational cost, similar DFT calculations for the other three molecules investigated experimentally (HDT, AOT et DDT) were not carried out. This is why shorter chain lengths were investigated in our DFT models compared to the molecules used in experiments, although the anchoring groups and the tail groups were kept identical.

Effect of the chain length. For a given tail group, the chain length has been varied from four carbons (MPA, ΔWF =−0.48 eV) to 16 carbons (MHDA, ΔWF =−0.27 eV): the WF is shifted of 0.21 eV. This agrees with the early results from Evans and Ulman.[65] It shows the longer the chain length, the smaller the WF modification. Actually, this trend is confirmed by the experiments as shown on Figure 8-a, if DDT is excluded once again. The four molecules are represented in the order of increasing chain length from C_6 to C_{16} and ΔWF decreases. The WF modification is of 0.29 eV here. With a longer chain, the molecule can accommodate more easily the local charges and decrease the resulting electrostatic dipole. Interestingly, calculations from Tong *et al.* at a lower molecule coverage, show that longer chains induce an increase of the WF[44] in contrast with our calculations at coverages close to saturation. At higher coverage, the lateral interactions between molecules inside a SAM are stronger. This mutual interaction drastically affects the WF. Indeed, a recent theoretical study showed that the interchain energy has a leading impact on the stability of the SAM as a function of the chain length.[41] The important result here, is that changing the molecular chain length from C_6 to C_{16} accounts for a significant WF decrease of *ca* 0.25 eV, much larger than the systematic experimental uncertainty.

The case of DDT. Figure 8-a shows that DDT behaves very differently in some experiments. It exhibits a very strong ΔWF of −0.97 eV in agreement with the available literature.[5, 34, 35] The specificity of DDT comes from synergistic effects: a higher compacity of the SAM leading to higher coverage, and the absence of a hydrogen-bond network between the tail groups. According to our DFT results, both concomitant effects lead to a decrease of the WF. Since they do not take place in the SAM of DDT, this explains why its WF change reaches −1.0 eV.

The nature of the tail group. Four different tail groups were considered in our DFT models with the same chain length of C_4 (Figure 8-b). BDT is a non-polar molecule and exhibits the smallest WF decrease (−0.38 eV). ABT and MPA are the most polar ones and they induce the largest ΔWF (−0.49 eV and −0.48 eV, respectively). This confirms that the dipole moment of the molecule plays a role in the final value of the WF.[23] It corresponds to a contribution of −0.1 eV which is smaller than the contribution of the chain length. This 0.1 eV is in sharp contrast with the values of the electric dipole of the free molecules that were computed to +0.49 D and −5.25 D for ABT and MPA, respectively. We can conclude here that the nature and the polarity of the tail group has a rather limited influence on the final WF change when SAMs are elaborated on Au(111), which agrees with the conclusions from Ref.[43] on SAMs of bipyrimidine and from Ref.[66] where the tail dipolar group is flipped thanks to the azobenzene photoisomer.

Impact of the hydrogen bond network on the WF of the SAM. Finally, in the case of the MHDA molecule, we have shown that the long C_{16} chains provides flexibility to the COOH tail groups which eventually assemble through a complex hydrogen bond network (see Figure 6-e). Those additional bonds induce disordering in the SAM, which leads to a spreading the electric charge, and to a reduction of the surface molecular dipole. One can conclude that the charge distribution may be more uniform, thus reducing the resulting dipole moment. The strong impact of the disordering inside the SAM on the WF of the surface is also confirmed by recent publications.[22, 67]

Conclusions

We have investigated how the SAMs of families of thiol molecules affect the WF of Au(111), by using both theoretical and experimental techniques. First, the WF of the clean reconstructed Au(111) strongly depends on the environment; it is predicted at 5.26 eV in vacuum and detected at 5.1 eV by UPS in an UHV chamber (3 x 10^{-6} mbar) and at 4.87 eV in air. The adsorption of a SAM with a thiol anchoring group systematically induces a significant decrease of the WF from 0.97 eV to 0.30 eV, which is hardly predictable based on the value of the dipolar moment of the isolated molecule. Even the MHDA molecule, which has a strong inwards dipole, induces a decrease of the WF of 0.30 eV (calculated at 0.27 eV by DFT). From our results, we show that the largest impact on the WF change is due to the chain length (contribution of 0.2 eV), where the longer the

chain, the smaller the WF modification. Then, the nature of the tail group contributes at a lesser extent, ~0.1 eV, with the largest influence assigned to the carboxy moiety, then amino, methyl and thio groups. We also demonstrated the strong influence of the hydrogen bonding network between the tail groups at the surface of the SAM, as demonstrated by our DFT calculations for the case of MHDA. These hydrogen bond networks tend to smear out the charge localization and reduce the dipole contribution. This effect results in the lowest value of $\Delta WF = -0.30$ eV for MHDA (dense network of hydrogen bonding between the COOH moieties) and $\Delta WF = -0.97$ eV for DDT (no hydrogen bonding).

Conflicts of interest

The authors do not declare any conflict of interest.

Acknowledgements

The authors thank PSMN in Lyon and GENCI national resources (IDRIS, CINES, TGCC, project 609) for CPU time and assistance. The authors thank the CPER/SYSPROD 2015-2022 project (N°2019-AURA-P5B) and AXELERA Pôle de Compétitivité (PSMN Data Center).
KPFM acquisitions were carried out at the Advance Atomic Force Microscopy platform (advAFM) of Sorbonne Université.

Notes and references

1. E. E. Bedford, S. Boujday, V. Humblot, F. X. Gu and C.-M. Pradier, *Colloids and Surfaces B: Biointerfaces*, 2014, **116**, 489-496.
2. M. Sánchez-Molina, A. Díaz, E. Sauter, M. Zharnikov and J. M. López-Romero, *Appl. Surf. Sci.*, 2019, **470**, 259-268.
3. R. W. Zehner, B. F. Parsons, R. P. Hsung and L. R. Sita, *Langmuir*, 1999, **15**, 1121-1127.
4. B. de Boer, A. Hadipour, M. M. Mandoc, T. van Woudenbergh and P. W. M. Blom, *Advanced Materials*, 2005, **17**, 621-625.
5. L. F. N. Ah Qune, H. Akiyama, T. Nagahiro, K. Tamada and A. T. S. Wee, *Appl. Phys. Lett.*, 2008, **93**, 083109.
6. N. Crivillers, S. Osella, C. Van Dyck, G. M. Lazzerini, D. Cornil, A. Liscio, F. Di Stasio, S. Mian, O. Fenwick, F. Reinders, M. Neuburger, E. Treossi, M. Mayor, V. Palermo, F. Cacialli, J. Cornil and P. Samorì, *Advanced Materials*, 2013, **25**, 432-436.
7. S. Casalini, C. A. Bortolotti, F. Leonardi and F. Biscarini, *Chemical Society Reviews*, 2017, **46**, 40-71.
8. W. E. Ford, D. Gao, N. Knorr, R. Wirtz, F. Scholz, Z. Karipidou, K. Ogasawara, S. Rosselli, V. Rodin, G. Nelles and F. von Wrochem, *ACS Nano*, 2014, **8**, 9173-9180.
9. M. Ochs, L. Jucker, M. Rödel, M. Emmerling, R. Kullock, J. Pflaum, M. Mayor and B. Hecht, *Nanoscale*, 2023, **15**, 5249-5256.
10. C. Vericat, M. Vela, G. Benitez, P. Carro and R. Salvarezza, *Chemical Society Reviews*, 2010, **39**, 1805-1834.
11. D. Woodruff, *Phys. Chem. Chem. Phys.*, 2008, **10**, 7211-7221.
12. J. C. Love, L. A. Estroff, J. K. Kriebel, R. G. Nuzzo and G. M. Whitesides, *Chemical Reviews*, 2005, **105**, 1103-1170.
13. Q. Guo, X. Sun and R. E. Palmer, *Physical Review B*, 2005, **71**, 035406.
14. L. Müller-Meskamp, B. Lüssem, S. Karthäuser and R. Waser, *The Journal of Physical Chemistry B*, 2005, **109**, 11424-11426.
15. H. Guesmi, N. B. Luque, E. Santos and F. Tielens, *Chemistry – A European Journal*, 2017, **23**, 1402-1408.
16. P. Feulner and M. Zharnikov, *Journal of Electron Spectroscopy and Related Phenomena*, 2021, **248**, 147057.
17. S.-H. Lee, W.-C. Lin, C.-J. Chang, C.-C. Huang, C.-P. Liu, C.-H. Kuo, H.-Y. Chang, Y.-W. You, W.-L. Kao, G.-J. Yen, D.-Y. Kuo, Y.-T. Kuo, M.-H. Tsai and J.-J. Shyue, *Phys. Chem. Chem. Phys.*, 2011, **13**, 4335-4339.
18. S. Techane, D. R. Baer and D. G. Castner, *Analytical Chemistry*, 2011, **83**, 6704-6712.
19. V. Y. Kutsenko, Y. Y. Lopatina, L. Bossard-Giannesini, O. A. Marchenko, O. Pluchery and S. Snegir, *Nanotechnology*, 2017, **28**, 235603-235610.
20. J. K. Roy, E. S. Vasquez, H. P. Pinto, S. Kumari, K. B. Walters and J. Leszczynski, *Phys. Chem. Chem. Phys.*, 2019, **21**, 23320-23328.
21. A. Asyuda, A. Wiesner, X. Wan, A. Terfort and M. Zharnikov, *J. Phys. Chem. C*, 2020, **124**, 24837-24848.
22. H. Kang, S. Seong, E. Ito, T. Isoshima, M. Hara, H. J. Yoon and J. Noh, *Appl. Surf. Sci.*, 2021, **555**, 149671.
23. S. Das, F. Ishiwari, Y. Shoji, T. Fukushima and M. Zharnikov, *J. Phys. Chem. C*, 2023, **127**, 2088-2097.
24. G. Heimel, L. Romaner, E. Zojer and J.-L. Brédas, *Nano Letters*, 2007, **7**, 932-940.
25. D. A. Egger, F. Rissner, G. M. Rangger, O. T. Hofmann, L. Wittwer, G. Heimel and E. Zojer, *Phys. Chem. Chem. Phys.*, 2010, **12**, 4291-4294.
26. O. M. Cabarcos, S. Schuster, I. Hehn, P. P. Zhang, M. M. Maitani, N. Sullivan, J.-B. Giguère, J.-F. Morin, P. S. Weiss, E. Zojer, M. Zharnikov and D. L. Allara, *J. Phys. Chem. C*, 2017, **121**, 15815-15830.
27. R. C. Bruce, L. You, A. Förster, S. Pookpanratana, O. Pomerenk, H. J. Lee, M. D. Marquez, R. Ghanbaripour, O. Zenasni, T. R. Lee and C. A. Hacker, *J. Phys. Chem. C*, 2018, **122**, 4881-4890.
28. E. Zojer, A. Terfort and M. Zharnikov, *Accounts of Chemical Research*, 2022, **55**, 1857-1867.
29. F. J. Himpsel, G. Hollinger and R. A. Pollak, *Physical Review B*, 1983, **28**, 7014-7018.
30. A. Kahn, *Materials Horizons*, 2016, **3**, 7-10.
31. K. Wong, S. Vongehr and V. V. Kresin, *Physical Review B*, 2003, **67**, 035406.
32. P. A. F. Garrillo, B. Grevin, N. Chevalier and L. Borowik, *Review of Scientific Instruments*, 2018, **89**.
33. E. Sauter, A. Terfort and M. Zharnikov, *J. Phys. Chem. C*, 2020, **124**, 28596-28604.
34. K. T. Narasimha, C. Ge, J. D. Fabbri, W. Clay, B. A. Tkachenko, A. A. Fokin, P. R. Schreiner, J. E. Dahl, R. M. K. Carlson, Z. X. Shen and N. A. Melosh, *Nature Nanotechnology*, 2016, **11**, 267-272.
35. H. J. Lee, A. C. Jamison and T. R. Lee, *Accounts of Chemical Research*, 2015, **48**, 3007-3015.
36. G. Heimel, L. Romaner, E. Zojer and J.-L. Bredas, *Accounts of Chemical Research*, 2008, **41**, 721-729.
37. G. Heimel, I. Salzmann, S. Duhm and N. Koch, *Chemistry of Materials*, 2011, **23**, 359-377.
38. V. Diez-Cabanes, D. C. Morales, M. Souto, M. Paradinas, F. Delchiaro, A. Painelli, C. Ocal, D. Cornil, J. Cornil, J. Veciana and I. Ratera, *Adv. Mater. Technol.*, 2019, **4**, 1800152.
39. G. Heimel, F. Rissner and E. Zojer, *Advanced Materials*, 2010, **22**, 2494-2513.
40. E. Mete, M. Yortanlı and M. F. Danışman, *Phys. Chem. Chem. Phys.*, 2017, **19**, 13756-13766.
41. A.-J. Truyens, J. Vekeman and F. Tielens, *Surface Science*, 2020, **696**, 121597.
42. E. Pensa, L. M. Azofra, T. Albrecht, R. C. Salvarezza and P. Carro, *J. Phys. Chem. C*, 2020, **124**, 26748-26758.

43. M. Gärtner, E. Sauter, G. Nascimbeni, A. Wiesner, M. Kind, P. Werner, C. Schuch, T. Abu-Husein, A. Asyuda, J. W. Bats, M. Bolte, E. Zojer, A. Terfort and M. Zharnikov, *J. Phys. Chem. C*, 2020, **124**, 504-519.
44. Y. Tong, G. R. Berdiyorov, A. Sinopoli, M. E. Madjet, V. A. Esaulov and H. Hamoudi, *Sci Rep*, 2021, **11**, 12772.
45. D. M. Kolb, A. S. Dakkouri and N. Batina, in *Nanoscale Probes of the Solid/Liquid Interface*, eds. A. A. Gewirth and H. Siegenthaler, Springer Netherlands, Dordrecht, 1995, DOI: 10.1007/978-94-015-8435-7_15, pp. 263-284.
46. C. Vaz-Domínguez, A. Aranzábal and A. Cuesta, *J. Phys. Chem. Lett.*, 2010, **1**, 2059-2062.
47. C. Maheu, L. Cardenas, E. Puzenat, P. Afanasiev and C. Geantet, *Phys. Chem. Chem. Phys.*, 2018, **20**, 25629-25637.
48. A. W. Dweydari and C. H. B. Mee, *physica status solidi (a)*, 1975, **27**, 223-230.
49. G. N. Derry, M. E. Kern and E. H. Worth, *Journal of Vacuum Science & Technology A*, 2015, **33**.
50. G. Kresse and J. Hafner, *Physical Review B*, 1993, **47**, 558-561.
51. G. Kresse and J. Furthmüller, *Physical Review B*, 1996, **54**, 11169-11186.
52. G. Kresse and J. Furthmüller, *Computational Materials Science*, 1996, **6**, 15-50.
53. J. P. Perdew, K. Burke and M. Ernzerhof, *Physical Review Letters*, 1996, **77**, 3865-3868.
54. S. Grimme, J. Antony, S. Ehrlich and H. Krieg, *The Journal of Chemical Physics*, 2010, **132**.
55. G. Kresse and D. Joubert, *Physical Review B*, 1999, **59**, 1758-1775.
56. W. Melitz, J. Shen, A. C. Kummel and S. Lee, *Surface Science Reports*, 2011, **66**, 1-27.
57. M. Uda, Y. Nakagawa, T. Yamamoto, M. Kawasaki, A. Nakamura, T. Saito and K. Hirose, *Journal of Electron Spectroscopy and Related Phenomena*, 1998, **88-91**, 767-771.
58. E. G. Castanon, A. Fernández Scarioni, H. W. Schumacher, S. Spencer, R. Perry, J. A. Vicary, C. A. Clifford and H. Corte-León, *Journal of Physics Communications*, 2020, **4**, 095025.
59. J. W. Kim and A. Kim, *Current Applied Physics*, 2021, **31**, 52-59.
60. L. J. Brillson, *Journal of Vacuum Science and Technology*, 1978, **15**, 1378-1383.
61. J. A. van Bokhoven and J. T. Miller, *J. Phys. Chem. C*, 2007, **111**, 9245-9249.
62. A. Kahn, N. Koch and W. Y. Gao, *Journal of Polymer Science Part B-Polymer Physics*, 2003, **41**, 2529-2548.
63. Y. Gao, *Materials Science and Engineering: R: Reports*, 2010, **68**, 39-87.
64. G. V. Hansson and S. A. Flodström, *Physical Review B*, 1978, **18**, 1572-1585.
65. S. D. Evans and A. Ulman, *Chemical Physics Letters*, 1990, **170**, 462-466.
66. S. Schuster, M. Füser, A. Asyuda, P. Cyganik, A. Terfort and M. Zharnikov, *Phys. Chem. Chem. Phys.*, 2019, **21**, 9098-9105.
67. D. Scaini, F. Biscarini, L. Casalis and C. Albonetti, *Chemical Physics Letters*, 2022, **803**, 139819.